NASA TECHNICAL NOTE

NASA TN D-4941

AN IMPACT ENERGY-ABSORBING STRUT EMPLOYING TUBE CUTTING

by Robert W. Warner and Arthur G. Kaskey

Ames Research Center
Moffett Field, Calif.

NATIONAL AERONAUTICS AND SPACE ADMINISTRATION • WASHINGTON, D. C. • DECEMBER 1968

NASA TN D-4941

AN IMPACT ENERGY-ABSORBING STRUT EMPLOYING TUBE CUTTING

By Robert W. Warner and Arthur G. Kaskey

Ames Research Center
Moffett Field, Calif.

NATIONAL AERONAUTICS AND SPACE ADMINISTRATION

For sale by the Clearinghouse for Federal Scientific and Technical Information
Springfield, Virginia 22151 – CFSTI price $3.00

AN IMPACT ENERGY-ABSORBING STRUT

EMPLOYING TUBE CUTTING

By Robert W. Warner and Arthur G. Kaskey

Ames Research Center

SUMMARY

An experimental evaluation is described for a tubular, nontelescoping, pin-ended strut that absorbs impact energy by tube cutting. Since this strut is shorter than a two-part telescoping strut, it offers a means for reducing the weight of any energy-absorbing truss (or other structure) in which a short strut is appropriate. The cutting load is reasonably constant over the stroke and repeatable for the impact velocities tested, which ranged from 3.0 to 11.9 feet per second, and for variations in impact weight, stroke length, and precutting. The lower and more meaningful of the two specific energy absorptions evaluated herein (5893 ft-lb per lbm) is obtained by dividing the product of the mean cutting load and the maximum possible stroke by the total strut weight (including end fittings). When modified in overall strut length, material, and number of cutters, as a check on adaptability, the system continued to function successfully.

INTRODUCTION

A large body of research has been conducted on mechanisms designed to fail and thereby absorb energy in a variety of impact situations, including the landing of space vehicles (e.g., refs. 1-6). For the type of mechanism placed inside a landing gear strut, weight has been reduced almost to the vanishing point. Therefore, further attempts at reducing weight should be directed toward the entire strut or even the entire landing gear truss.

Pin-ended struts for absorbing impact energy are either nontelescoping or telescoping. Because of the complexity of multiple systems, the struts considered here are restricted to two-part systems having a single ram and a single casing. Two prominent examples of telescoping struts are the system of reference 1, in which a wire hoop is worked by rolling it between a tubular casing and a telescoping ram; and the semicantilever system of reference 2, in which a ram crushes a core of honeycomb inside the tubular casing. For the same stroke and force, the telescoping strut tends to be the heavier because it requires a ram somewhat longer than the stroke length.

In nontelescoping struts, on the other hand, the ram length can be greatly reduced because the tubular strut casing is shortened by deformation during the stroke. To take advantage of the resulting reduction in weight,

however, the short ram itself must be lightweight. The casing may or may not contain a core of crushable material, such as honeycomb or balsa, to absorb additional energy.

For certain landing vehicles, such as the Lunar Excursion Module (LEM) discussed in reference 2, a long telescoping strut fits naturally into a lightweight truss design. For other designs it will be advantageous to use the shorter and potentially lighter nontelescoping strut. Several existing devices could be used, with appropriate modification, as nontelescoping struts with lightweight rams. These include a tube local buckling system (ref. 3), a tube-splitting system (ref. 4), and a tube-cutting system (ref. 5).

The pin-ended, nontelescoping, tube-cutting strut evaluated in this report differs from that of reference 5 in that during the energy-absorbing stroke, the tubular casing is cut into strips, which curl as the strut shortens. This process and tube splitting share an advantage over tube local buckling in that the deformation starts at a specified tube location and does not interfere with any auxiliary crushable energy absorber that might be used inside the strut.

The experimental evaluation of the present system is based on drop tests to measure energy absorption, mean cutting force, and deviation from a rectangular load-displacement curve. Repeatability and the effects of impact velocity, stroke, impact weight, and precutting are checked. Several modifications of the present system are briefly evaluated.

NOTATION

A	cross-sectional area of tube material
D_i	tube inside diameter
E	modulus of elasticity
F	tube buckling load, local or bending
F_{max}	maximum value of F
F_c	mean cutting force, based on a time average
K	end fixity factor for bending buckling
L	overall strut length, including balls of two ball joints
R	mean radius of tube
SEA_o	$\frac{F_c s_{max}}{w_s}$

SEA_t $\dfrac{F_c s_{max}}{w_t}$

s_{max} maximum possible stroke, terminated by contact between end fittings

t tube wall thickness

w_s total strut weight (see table II)

w_t tube weight

γ load-constancy factor, that is, ratio of maximum cutting force (without noise) to mean cutting force during stroke

TEST EQUIPMENT AND PROCEDURE

Component parts of the model are shown in figures 1 to 3, and figure 4 is a photograph of a nearly static test arrangement used in preliminary cutting and buckling tests. The cutting end of the final assembled model is shown in figure 5. The entire model is shown in figure 6 prior to a drop test, together with the drop-test apparatus and instrumentation.

Model

The model (fig. 6) is a pin-ended strut consisting of a tube with a ball at each end, a cutting dome between the tube and one ball, and a noncutting dome between the tube and the other ball. In the development of this model, an attempt has been made to achieve a maximum buckling load per unit of model weight. This provides a large margin of safety between buckling and cutting. The model development (appendix A) utilizes the nearly static test arrangement of figure 4 as well as drop tests and buckling formulas.

The two most important components of the model are the tube and the cutting dome. The tube of figures 5 and 6 is 18 inches long, giving an overall strut length of 21.75 inches (including the balls of the ball fittings). The tube was machined from commercial drawn tubing, 2024-T3 aluminum alloy (hard), having an inside diameter of 1.87 inches, an outside diameter of 2 inches, and a wall thickness of 0.065 inch. The machining reduced the wall thickness to 0.0357 inch and the outside diameter to 1.9414 inches while retaining the inside diameter of 1.87 inches. After machining, the tube inner-surface hardness measured 112.7 on the Rockwell H scale and the tube ultimate tensile strength measured 69,000 psi (to be compared to a Rockwell H measurement of 114.7 and a tensile strength measurement of 70,200 psi prior to machining, as well as a typical tensile strength of 70,000 psi from ref. 7).

The cutting dome (figs. 2 and 5) consists of a dome head, a cutter ring, and a skirt. The skirt, which fits inside the tube to guide the cutting action (fig. 2), was machined from 2024-T4 aluminum alloy (having a typical ultimate tensile strength of 68,000 psi according to ref. 7), as was the dome

head. Dimensions are given in figure 2 for the dome head, which contains holes to prevent air compression from contributing to the energy absorption.

As shown, the cutter ring fits onto the base of the dome head and is fastened when the skirt is screwed in place. The ring, with details shown in figure 1, was made from 4340 steel by an electrical discharge process. It has 20 integral cutters, each with a rectangular cutting surface swept back 15° from a normal to the cutting direction. The hardness of the cutters was measured as 76.5 on the Rockwell A scale (equivalent to 51 on the C scale).

The noncutting dome (figs. 3 and 6) is similar to the cutting dome except that it lacks cutters and has a shorter skirt. Its main function is to transfer impact load to the tube from the impact ball in the drop-test arrangement (fig. 6). In general, the noncutting dome was used at both ends of the tube in all (preliminary) buckling tests and at one end in all cutting tests, whether nearly static or dynamic.

The balls shown in figures 4, 5, and 6 are 1 inch in diameter, and each has a flat spot where it is bolted to the dome. To permit repeated testing, the balls are made of 4340 steel, but for a one-shot landing, aluminum balls would be adequate.

Before the models were assembled, the outside of the cutting dome skirt and the inside of the tube were sprayed with a fluorocarbon dry lubricant. When assembled, the tube was held lightly against the cutters by rubber bands attached to the inside of the loading domes.

The cutting model described in this subsection is the basic model for the present tests. Certain variations tested to determine the adaptability of the system will be described when their results are reported.

Apparatus and Instrumentation

The apparatus for the final drop tests consists of the drop hammer table, shown in figure 6, together with its hoist cable and guide rails, the simulated truss, the sockets, and the retainer ring (fig. 5). The simulated truss originally was intended to evaluate the possible binding (which did not occur) of the cut strips of tubing against such a truss (fig. 7). For the preliminary nearly static tests, the drop hammer system was replaced by a servo hydraulic load frame (such as that shown in fig. 4), and the retainer ring was removed.

The quantities measured were force, displacement, and time, from which impact velocity was deduced. A Bytrex load cell (model JP-10KD), having a capacity of 10,000 lb for static and dynamic loads, was used to measure force. This load cell (fig. 6) converts force to voltage by means of a Wheatstone bridge consisting of semiconductor strain gages bonded to a high strength member.

In the drop tests displacement was measured by a Research, Inc., 5-foot potentiometer-type displacement transducer, model 4040, and also by high-speed

movies of a pointer on the hammer table moving over the 1-inch strips shown in figure 6. The speed of the high-speed movies was 400 frames/second. For the static tests, displacement was measured by the displacement element of the x-y plotter associated with the hydraulic loading frame and also by a separate potentiometer (different from the one used for the drop tests).

Time was measured by a timing light recorded on the movie film at 120 pulses/second and also by timing lines recorded on the recording oscillograph paper at 100 lines/second.

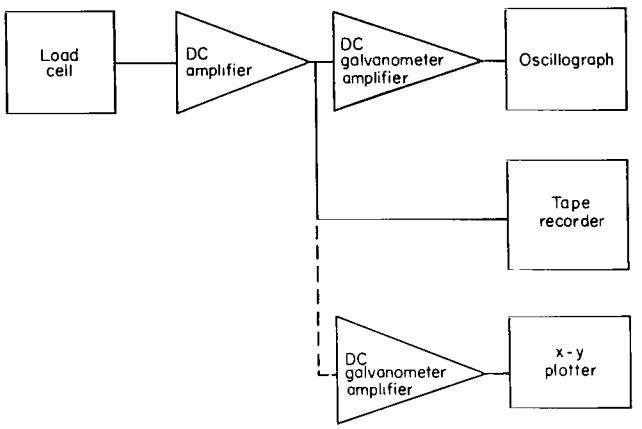

Sketch (a)

Sketch (a) is a block diagram of the force instrumentation (both primary and recording). The load cell signal was amplified and then recorded on both the oscillograph and the tape recorder during the drop tests, and on the x-y plotter during the static tests. The load cell was powered by batteries to eliminate ripple in the records.

The force instrumentation was calibrated with the aid of proving rings of various capacities calibrated by the U.S. Bureau of Standards. The effects of drift in amplifier gain and battery voltage were accounted for by electrical calibrations at the beginning and end of each test sequence. These calibrations utilized a resistance in parallel with an inactive leg of the bridge, which gave an output reading corresponding to a known load when switched into the circuit.

The displacement instrumentation was similar to that shown in sketch (a) except that a potentiometer-type displacement transducer was used instead of the load cell. The electrical calibration modified the potentiometer resistance (rather than a strain gage leg), and the calibrating standard was a steel scale (rather than a proving ring). The displacement calibration was double-checked by measuring several of the total tube cutting or buckling strokes with a steel scale and comparing the results with the stroke length determined by the oscillograph readings. The worst error was 1 percent.

Test Procedure and Estimate of Impact Velocities

In general, typical procedures for static load and drop tests were followed. For the drop tests, lead weights were placed on top of the hammer table to give the desired stroke into the tube. Drop heights were 3, 12, and 27 inches, as shown in table I, giving free-fall impact velocities of 4, 8, and 12 ft/sec, respectively. More accurate velocities were calculated by equating impact kinetic energy and work based on the impact weights, strokes, and mean cutting forces, F_c of table I (neglecting friction during impact).

The resulting impact velocities, as reported in table I, were somewhat less than the nominal free-fall values, possibly because of binding of the drop hammer rollers in their vertical channels at the start of the drops.

As a check on impact velocity, displacement time histories were plotted on the basis of the high-speed movies. The greatest discrepancy between velocities deduced from these time histories and the calculated impact velocities of table I (based on energy) was 6.3 percent for case 13; the value in table I is considered the more accurate. Velocities determined from the movie time histories seem more accurate than those from the oscillograph time histories (fig. 8). The latter velocities, often unrelated to the strokes, were sometimes greater than gravity would permit (probably because of a small range for displacement on the oscillograph paper).

RESULTS AND DISCUSSION

Static and drop tests were used in developing the tube-cutting system, but the evaluation to be reported in this section is based on drop tests only. Preliminary tests were made to insure that the segments into which the tube was cut would not interfere with a truss member or vehicle base. It was found that the cutters, in moving down through the tubular casing, curled the tube segments back so tightly that they did not even touch the ridge intended to spread them (fig. 7) and would obviously clear a horizontal truss member or vehicle base.

Effects of Impact Velocity, Stroke, Impact Weight, and Precutting

The effects of impact velocity, stroke, weight, and precutting on the mean cutting force are summarized in table I.[1] The values reported for maximum cutting force and for the entire force time history exclude noise in the output signals caused by ringing of the mechanical system (drop hammer, model, load cell), which is typical of any device that produces a square-wave loading. It is apparent in table I that for the range of impact velocities and weights shown, with a corresponding range of stroke, the variation in mean cutting force F_c is insignificant. This is true regardless of whether the tube was precut (by a short drop). Similarly (again excluding noise, and hence any high-frequency initial peak), there is no significant effect on the γ values in table I of the indicated variations in impact velocity, stroke, impact weight, and precutting. The slight trend toward increasing γ as the impact velocity decreases is too small to be validated without additional data. This is an important result, since γ is the ratio of the maximum cutting force to the mean cutting force. The maximum cutting force, together with the vehicle mass, determines the maximum vehicle deceleration; and the mean cutting force, together with the stroke, closely approximates the impact energy absorbed (provided the cutting force is nearly constant).

[1]The mean cutting force F_c is taken to be the time average over the stroke time considered. The stroke time does not include the time in which the force builds up to, or drops off from, the relatively constant cutting force shown in figure 8.

Repeatability and Magnitude for γ and F_c

Since none of the parameters varied in table I had any important effect on γ or F_c, all cases are considered in evaluating repeatability and magnitude. Repeatability is measured by the ratios of the standard deviations to the ensemble mean values recorded at the bottom of table I. These ratios are well below 0.05 for γ and F_c, suggesting excellent repeatability. With respect to magnitude, the maximum value of γ, 1.160, and the ensemble mean value of 1.081 indicate a nearly constant cutting force.

The ensemble mean value of F_c shown in table I as 3,273.6 lb is roughly one-third of the 10,000 lb experimental buckling load (see appendix A) and seems low. However, if energy were absorbed by buckling, it would be absorbed at the postbuckling load rather than the buckling load; and the postbuckling load for the present tubes ranges from one-third to two-thirds of the cutting load (where post bending buckling crimped the tubes and where post local buckling split the tubes in the present tests).

The 10,000-lb load is for a maximum buckling load configuration (see appendix A) and provides the maximum or very nearly the maximum margin of safety between the cutting and buckling loads. At the expense of this safety factor, the present tube could have been lengthened until its lesser buckling load (bending, for the longer tube) was lowered to the limit of safety. This would make the cutting and lesser buckling loads nearly equal, and would increase the overall specific energy absorption of the entire strut for cutting.

Specific Energy Absorption

The value of SEA_o, the overall specific energy absorption reported in table II, assumes that the cutting load is so nearly constant that the mean load based on time is nearly the same as that based on displacement. The two mean loads were found to differ by 2 percent for case 9 in table I, which has one of the least constant time histories. Figure 8(d) is the time history for case 9; and figure 9 is the corresponding plot of cutting load versus displacement.

The value of SEA_o found in these tests was 5,893 ft-lb/lbm. Although this may appear unduly small, it must be remembered that the weight employed was the total strut weight. For applications other than struts, it is more common to consider only the gross weight, in this case the tube weight, of the item to be crushed or otherwise deformed. With the energy absorption unchanged, the tube weight defines a second specific energy absorption, SEA_t, which for these tests was the much higher value (given in table II) of 10,950 ft-lb/lbm.

A comparison of the SEA_t of 10,950 ft-lb/lbm with the value of 24,000 ft-lb/lbm deducible for balsa, one of the very best absorbers (ref. 8), suggests that for nonstrut applications balsa is a better energy absorber than tube cutting. For struts, however, particularly those as slender as the present one, the balsa would require a casing or guide rod of

undetermined weight to prevent buckling. Thus, the quantity SEA_t may well be meaningless for struts, and SEA_o should be used for future strut comparisons.

Adaptability

To determine the adaptability of the present system to changes in the basic strut design, several modifications were briefly evaluated in terms of their effect on the mean cutting force and general system functioning.

As indicated in table III, the material was changed from 2024-T3 to 3003-H14 aluminum alloy,[2] the number of cutters from 20 to 15 (with no other change in cutter configuration for table III), and the overall tube length (including end fittings) from 21.75 to 12.75 inches or 9.75 inches. Combination 1 (table III) is the basic configuration, and combinations 2 through 6 are modifications. The results for combination 1 constitute averages for 13 cases, of which 9 have precut tubes. The remaining combinations, all with precut tubes, generally represent fewer cases per combination.

The cutting system functioned satisfactorily for all modifications. However, the γ values are often somewhat higher for combinations 2 through 6 than for combination 1, indicating a higher maximum force for a given energy absorption (mean force). It should also be noted that the 15-cutter configuration would require a spreader ridge somewhat larger than that shown in figure 2 if the cut strips of tubing are required to curl as tightly as in figure 7. (The spreader ridge is not required for a 20-cutter configuration.)

With respect to cutting force, successive combinations are compared as pairs in table III (1 with 2, 3 with 4, and 5 with 6); and length is the only parameter changed within a pair. Except for combinations 5 and 6, these length changes resulted in no significant change in cutting force, as seen in table III. Since combination 6 is the only one for which the length is as low as 9.75 inches, it is possible that length has a slight effect for very short tubes.

The remaining parameters in table III have the expected general effects on the mean cutting force, which increases with tube hardness and number of cutters. Since the present study was concerned primarily with the feasibility and adaptability of the system, the parametric variation was not carried far enough (particularly for the wall thickness, cutter sweep angle, and cutter width) to permit correlation with simplified theory.

The sharpening of the cutters on the 15- and 20-cutter ring not reported in table III is considered an auxiliary variation and is discussed with other auxiliary material in appendix B.

---

[2]For which the ultimate tensile strength was measured as 22,800 psi after machining, compared to 22,300 psi before machining and a typical value of 22,000 psi from reference 7.

Scaling and Other Unresolved Questions

The scaling data reported in appendix A suggest that geometric scaling is satisfactory for an unswept cutter of triangular cross section with a 30° included angle cutting edge. This requires that the model and prototype be made of the same material so that stresses and densities are unchanged. Then forces, except for weight, vary according to the square of a representative scaling dimension, and masses vary according to the cube. (See ref. 6 for more detail on geometric scaling.)

It seems reasonable that geometric scaling will apply for rectangular cutters as well as the triangular cutter for which scaling was checked. However, even the triangular cutter data (appendix A) leave much to be desired: they are based on strip testing rather than tube testing, show considerable scatter for a small number of tests, and were obtained for only one material (6061-T6 aluminum alloy). Scaling, therefore, must be listed as an unresolved question.

A second unresolved question is whether harder materials can profitably be used for cutting. This depends on whether the harder tubes would split catastrophically, a possibility not investigated in this project. Another question involves the feasibility of using tubes having the wall thickness tapered to increase the cutting load during the stroke (thereby helping to prevent vehicle tipover and, possibly, ringing). Questions also remain as to the effect on the cutting system of a space or rocket exhaust environment, from which a nontelescoping strut could be only partially protected without a major weight addition. The possible binding of a cutting system when high decelerations are applied in a direction not parallel to the axis of the strut must also be investigated. Finally, the effects of very high cutting velocities (hundreds of feet per second, as opposed to the maximum of roughly 12 ft/sec considered here) must be evaluated before the tube cutting arrangement investigated here can be considered for hard landings. (Successful results have been obtained at velocities up to 75 ft/sec in other tests.)

CONCLUDING REMARKS

A tubular, pin-ended strut for absorbing impact energy by tube cutting has been experimentally evaluated. Tube dimensions selected maximize the buckling load, thereby providing a large margin of safety between buckling and cutting. The basic cutter-tube combination was made primarily of hard aluminum alloy according to the following principal specifications: overall strut length, 21.75 inches; inside diameter, 1.87 inches; wall thickness, 0.0357 inch; number of rectangular cutters, 20; and sweep angle of cutting surface, 15°. For this basic strut the following conclusions apply:

1. The system proved physically feasible as a nontelescoping strut in that the cut tube segments curled tightly during the energy-absorbing stroke, thereby shortening the strut and avoiding potential interference with another structure (such as the space vehicle body or the rest of the landing gear truss).

2. Neither the mean cutting force nor the load constancy factor (maximum cutting force, without noise, divided by mean cutting force during stroke) was significantly affected by the following parametric variations: estimated impact velocities ranging from 3.0 to 11.9 ft/sec, stroke lengths from 0.509 to 11.375 inches, impact weights from 601 to 1003 lb, and precutting versus no precutting.

3. Repeatability was excellent for both the mean cutting force and the load constancy factor; the ratios of their standard deviations to ensemble means were well below 0.05 for 13 drop tests.

4. The cutting load was reasonably constant over the stroke, as indicated by the maximum load constancy factor of 1.160 and the ensemble mean of 1.081.

5. The lower and more meaningful of the two types of specific energy absorption, defined as the product of the mean cutting load and the maximum possible stroke divided by the total strut weight (including end fittings), was 5893 ft-lb/lbm.

6. When modified in overall length, material, and number of cutters as a check on adaptability, the system continued to function successfully.

Ames Research Center
National Aeronautics and Space Administration
Moffett Field, Calif., 94035, August 7, 1968
124-08-04-02-00-21

APPENDIX A

MODEL DEVELOPMENT

The model development is discussed in the order in which it occurred.

STRIP TESTING, INCLUDING SCALING EFFECTS

The initial phase of model development involved (nearly) static tests in which a load-displacement testing machine was used to pull a single cutter through a strip of metal (6061-T6 aluminum alloy). This "strip-test" approach was used, as opposed to the more realistic pushing of several cutters through a tube, to facilitate the changing of cutter shapes and material thicknesses. Except for scaling changes, only five cutters were tried: (1) a cutter of triangular cross section having a 30° cutting edge (included angle) swept back 9° from a normal to the direction of motion; (2) a similar cutter having a 0° sweep angle; (3) a triangular cutter having a 15° cutting edge and a 0° sweep angle; (4) a square cutter having a 9° sweep angle; and (5) a square cutter having a 15° sweep angle. The fifth, shown in figure 1, proved most nearly satisfactory with respect to force variation during the cutting stroke and with respect to repeatability.

As an auxiliary part of the strip-test program, a limited amount of scaling information was obtained for the unswept triangular cutter with a 30° cutting edge. A group of (four) tests with a 0.140-inch-wide cutter and a 0.036-inch-thick sheet yielded time-average cutting loads from 848 to 990 lb and an ensemble average cutting load of 895 lb. A second group of (three) tests with a 0.070-inch-wide cutter and a 0.0165-inch-thick sheet gave time-average loads from 166 to 231 lb with an ensemble average of 196 lb. The comparison of these two test groups gives geometric ratios of 2.0 for cutter width and roughly 2.2 for sheet thickness, together with a load ratio of roughly 4.6. This suggests geometric scaling, for which a geometric ratio of 2.0 should give a load ratio of $(2.0)^2$ or 4.0.

EIGHT-CUTTER TESTS

Eight of the swept cutters selected in the strip tests were arranged in a ring on a preliminary cutting ram. The ram was then pushed through several preliminary tubes by a simulated truss in a static test machine, and a replaceable system of spreaders on the ram was developed to spread the cut strips of tubing and prevent them from damaging the simulated truss. The first spreader system tried proved to be satisfactory for the 8-cutter ram. These tests provided information for the final spreader design of figure 2, in which the replaceable system becomes a nonreplaceable ridge on the cutter dome. The

final system, however, comprised 20 cutters instead of 8; and the 20 cutters spread and curled the tube strip segments so tightly that the spreader ridge was unnecessary.

A more rewarding result of the 8-cutter tests was the finding that the cutting load was far more repeatable than in the strip tests (probably because of the averaging of deviations among 8 cutters), and that the resulting repeatability made the cutting system qualitatively feasible.

SELECTION OF TUBE CROSS SECTION ACCORDING TO BUCKLING FORMULAS

The design of the final system depended on selection of the cross section for the final tubing. Ideally, the selection of tube cross section, together with all other tube and cutter dimensions, should be an integral part of an overall system design. However, the number of cutting tests required to validate an integrated design procedure was considered beyond the scope of the present investigation.

In the absence of an integrated cutting design procedure, tube selection was based on achieving a maximum buckling load for a given tube weight under end conditions consistent with those provided by the cutters. This permits the largest possible cutting load but does not, of course, guarantee that such a cutting load will be achievable with any existing cutters (the maximum permissible number and size of cutters being limited by tube splitting and the resulting load reduction). Even if the achievable cutting load is low, however, the tube selected for maximum buckling load retains the advantage of providing the maximum, or very nearly the maximum, margin of safety.

For determination of the tube cross section giving the maximum buckling load according to buckling formulas, it is assumed that the cross-sectional area A and the tube length L are fixed, thereby fixing the tube weight for any given material. Under this temporary assumption, the maximum buckling load can be pictured as in sketch (b), where F is the buckling load, D_i the tube inside diameter, and t the wall thickness. The maximum buckling load F_{max} is seen to occur at the ratio of inside diameter to wall thickness $(D_i/t)_{F_{max}}$, where the bending buckling and local buckling curves intersect (as suggested in ref. 9).

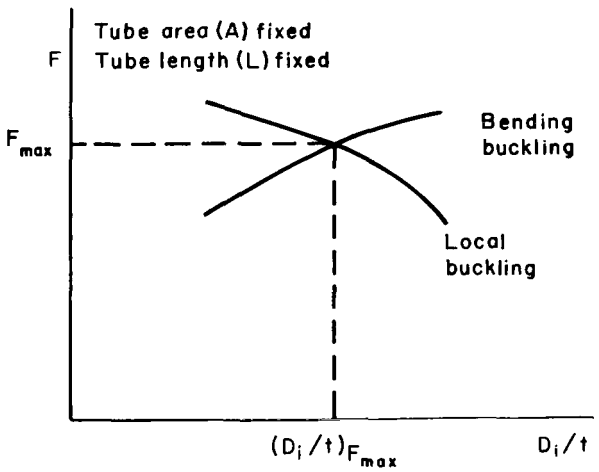

Sketch (b)

A locus of similar intersections was calculated for any aluminum alloy tube having a given effective length KL, where K is the end fixity factor for bending buckling, by equating the load formulas for bending buckling and local buckling given in reference 10. The locus has the form shown in

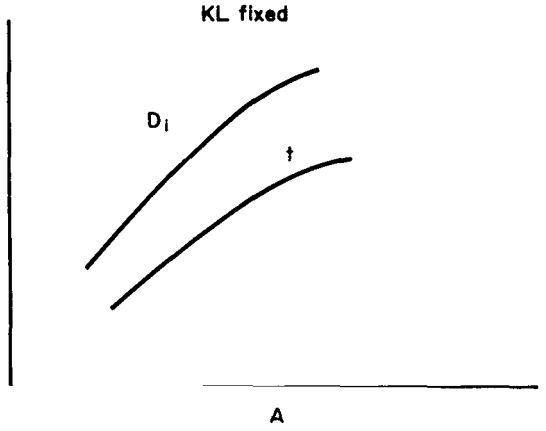

Sketch (c)

sketch (c). With KL selected in advance, the selection of either D_i, t, or A determines the other two. In the present case, KL was fixed (for analytical purposes) at 16 inches. With tubing available having D_i = 1.87 inches, the other two quantities were determined as t = 0.0357 inch and A = 0.2137 square inch. Thus the tube cross section has been specified for maximum buckling load, subject to the constraint of D_i = 1.87 inches. If desired, this maximum buckling load can be calculated according to either the bending or local buckling formulas of reference 10. A set of maximum load calculations could be used to construct buckling design charts for which F_{max} and L are given and the minimum A is to be determined with no constraint on D_i.

DESIGN OF END-FITTING DOME WITHOUT CUTTERS

After the cross section was specified, it was possible to design the domes in the end fittings. The load for the domes was taken to be higher than the predicted tube buckling load because of stated conservatism in the buckling formulas of reference 10. The dome load initially determined was 10,700 lb, the product of the tube area and a typical yield stress for the selected tube material (2024-T3 aluminum alloy in ref. 7).

The dome without cutters (or noncutting dome) was designed first (fig. 3). It was made as lightweight as a rough design would permit. The material selected was 2024-T4 aluminum. With the skirt of 0.030-inch-thick material cut off, the dome was tested in a static test machine and found to fail at 18,900 lb.

MODIFICATION OF TUBE LENGTH ACCORDING TO BUCKLING EXPERIMENTS

Two of the noncutting domes were used in (nearly) static buckling tests of the tubes, for which the cross section had already been determined. To provide a nearly perfect pin end fixity, steel balls were bolted to the domes and fitted into steel sockets (fig. 4). The intersection illustrated in sketch (b) was found experimentally by noting, with the aid of buckling force measurements and moving pictures, the transition from local buckling to bending buckling as the tube length was increased over a range that spanned the predicted length of 16 inches (KL = 16 inches with K = 1 for pin-end fixity).

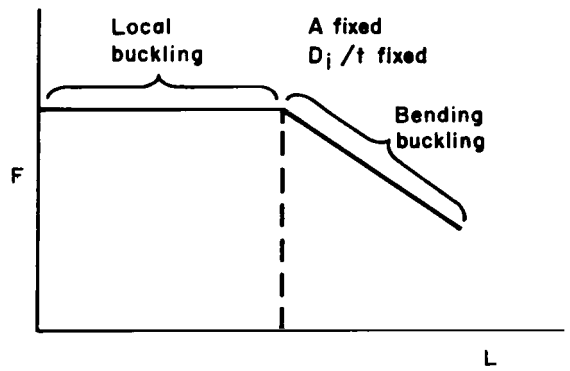

Sketch (d)

The buckling force F was plotted against tube length L as indicated in sketch (d), with A and D_i/t fixed according to the selected cross section. The abrupt change of slope in sketch (d) determined the transition between local buckling and bending buckling and thereby determined the value of L (L = 21.75 in.) for which the selected D_i/t is the $(D_i/t)_{F_{max}}$ defined in sketch (b). A corroboration of this value of L was found in the moving pictures. For L greater than 21.75 inches, the pictures showed that overall tube bending occurred and was followed by a crimp near the middle of the tube. For L less than 21.75 inches, however, a local buckling took place in which one end fitting or the other would cock, pulling the open end of the tube out of the round, doubling up the skin at that end over half a circumference, and finally splitting the skin.

This type of local buckling could occur if either free edge of the tube were loaded by a group of radial cutters and if the cutters failed to cut. In this sense the cutting end condition has been approximated for the buckling tests. It should also be noted that the local buckling region in sketch (d) does not necessarily have zero slope for end conditions different from the present ones and that these conditions are required if the presently selected tube dimensions are to provide a maximum buckling load.

For the end conditions under consideration, then, the buckling tests resulted in a tube length of 21.75 inches instead of the original length of 16 inches (with pin ends) selected for analytical purposes. For 21.75 inches, as well as all shorter lengths, the measured buckling load is roughly 10,000 lb. As expected, this is higher than the calculated value (measured load/calculated load = 1.16). The measured buckling load is, in fact, just under the typical yield load of 10,700 lb deduced from reference 7.

DESIGN OF END-FITTING DOME WITH CUTTERS

The measured buckling load of 10,000 lb is appreciably lower than the measured failure load reported earlier for the noncutting dome (18,900 lb). This suggests that the present strut is somewhat heavier than needed, although a lighter noncutting dome might have to accept a significant weight penalty for cutter attachment when converted to a cutting dome.

The steel cutter ring (fig. 1) was designed to be as light as possible. It was made by an electrical discharge process, and the sweep angle of the cutting surface was 15° (as determined in the preliminary tests). The ring was incorporated into a cutting dome (fig. 2). The main modification relative

to the noncutting dome was a longer tubular skirt to guide the cutting action. Rings were made with 15, 20, and 24 cutters. From these, the 20-cutter ring was selected as the final design since it gave the highest load in drop tests (the load being lower for 15 cutters because of reduced cutting area and for 24 cutters because of tube splitting).

APPENDIX B

AUXILIARY RESULTS AND DISCUSSION

RESULTS FOR SHARPENED CUTTERS

Some data were obtained when the 15- and 20-cutter rings were sharpened to a 60° included angle. In several drop tests with these configurations, the maximum cutting force was 6918 lb for a 2024-T3 tube of 0.0357-inch wall thickness with 20 cutters. Unfortunately, this large force occurred only at the end of the stroke, where the velocity was low. Not only were the sharp cutters highly rate dependent, they were also subject to much larger oscillations in cutting force than were the square cutters. If the force oscillations could be reduced, however, the sharp cutters might be useful in applications where rate dependence is needed to prevent tipover of the landing vehicle; but they were not investigated in depth during the present project.

EFFECT OF BALL JOINTS

It should be emphasized that the present strut was developed to operate between two ball joints and was tested under those conditions. Ball joints, as opposed to heavier hoop or ring fittings, do not permit the passage of strut material through the end fittings during the energy-absorbing stroke. Hence the present end fittings posed the requirement that the cut strips of tubing curl or be curled to avoid damage to the rest of the landing gear truss, a requirement which was readily met. An additional problem, inherent in any pin-end fitting, was the difficulty in preventing undesired bending buckling of the strut. However, the ball joints reduced the design problem in one sense, since no bending stresses were introduced except by buckling. The present design could readily be extended to permit the introduction of moderate bending stresses, such as those in the semicantilever design for LEM (ref. 2), although the effect on overall weight would require investigation.

ADVANTAGE ILLUSTRATED BY CATASTROPHIC FAILURES

Whether pin-end fittings have anything to do with the start of local buckling is not certain; once local buckling has started, however, pin-end fittings lead to catastrophic failure, as shown in figures 10 and 11. In both cases the cutter dome cocked and was pulled out of the tube, permitting the drop hammer to descend unobstructed. These catastrophic failures occurred when the number of cutters was increased to the point where cutting did not occur. Figure 10 illustrates the splitting type of local buckling encountered with the hard (2024-T3) aluminum alloy and figure 11 the splitting and crimping type experienced by the soft alloy (3003-H14).

These two failures illustrate an advantage of tube cutting over tube local buckling (including the case of splitting) as an energy absorber. This advantage is that a more effective (and probably heavier) guiding system is required for tube local buckling than for tube cutting to prevent catastrophic failure.

REFERENCES

1. Anon.: Concepts of Multiple-Impact Study of Energy Absorption. NASA CR-273, 1965.

2. Hilderman, Richard A.; Mueller, William H.; and Mantus, Morton: Landing Dynamics of the Lunar Excursion Module. J. Spacecraft Rockets, vol. 3, Oct. 1966, p. 1484.

3. Coppa, A. P.: Collapsible Shell Structures for Lunar Landings. ARS Preprint 2156-61, 1961.

4. Mitchell, Bruce: U. S. Patent No. 3,236,333; Energy Absorber, February 22, 1966.

5. Rayfield, J. F., et al.: U. S. Patent No. 2,961,204; Deceleration Device, November 22, 1960.

6. Warner, Robert W.; Sorenson, Robert M.; and Kaskey, Arthur J.: An Investigation of a Deforming Energy-Absorption System for Space-Vehicle Landings. NASA TN D-3061, 1965.

7. Anon.: Alcoa Aluminum Handbook. Aluminum Company of America, Pittsburgh, 1966.

8. Knoell, A. C.: Environmental and Physical Effects on the Response of Balsa Wood as an Energy Dissipator. Tech. Rep. 32-944, Jet Propulsion Laboratory, June 15, 1966.

9. Zahorski, Adam: Effects of Material Distribution on Strength of Panels. J. Aero. Sci., vol. 11, no. 3, July 1944, pp. 247-253.

10. Anon.: Alcoa Structural Handbook. Aluminum Company of America, Pittsburgh, 1960.

TABLE I.- TUBE PROPERTIES AND CUTTING LOAD RESULTS

Case	Precut (?)	Mean wall thickness, in.	Impact weight, lb	Stroke, in.	Mean cutting force, F_c, lb	Estimated impact velocity, ft/sec	Drop height, in.	Ratio of maximum cutting force (without noise) to mean cutting force, γ
1	Yes	0.0349	601	5.747	3216.0	11.6	27	1.035
2	Yes	.0354	805	8.058	3236.6	11.4	27	1.037
3	No	.0342	805	8.652	3235.1	11.8	27	1.065
4	No	.0353	1003	11.053	3248.9	11.5	27	1.077
5	Yes	.0351	801	8.502	3275.8	11.9	27	1.086
6	Yes	.0355	801	7.739	3405.3	11.6	27	1.033
7	Yes	.0347	1003	11.375	3313.0	11.9	27	1.074
8	Yes	.0349	601	2.820	3080.7	7.9	12	1.077
9	Yes	.0355	805	3.420	3267.7	7.5	12	1.154
10	Yes	.0350	801	3.632	3233.5	7.7	12	1.038
11	No	.0348	601	.565	3301.7	3.7	3	1.075
12	No	.0355	805	.509	3485.8	3.0	3	1.140
13	Yes	.0349	801	.750	3256.5	3.5	3	1.160
Ensemble mean		.0351			3273.6			1.081
Standard deviation		.0004			92.3			.043

Tube material: 2024-T3; tube length (including end fittings) 21.75 in.
Tube cross section: 1.87 in. ID × 0.0351 in. wall.

TABLE II.- WEIGHTS AND SEA RESULTS FOR TUBE CUTTING

Item	Description	Weight, lb
1	1 tube (no end fittings), 2024-T3, 18 in. long × 1.87 in. ID × 0.0351 in. wall	0.3936
2	1 cutting dome and skirt, 2024-T4	.1152
3	1 cutter ring (20 cutters), steel	.0284
4	1 noncutting dome and skirt, 2024-T4	.0932
5	2 balls, 2 screws, 2 washers with weight converted from steel to aluminum	.1003
	Total strut weight	.7307

Description of weight considered in SEA	Weight, lb	Ensemble mean of mean cutting force, lb	Maximum possible stroke, ft	SEA, ft-lb/lbm
Total strut (total of items 1-5 above)	0.7307	3273.6	1.316	$SEA_o = \frac{(3273.6)(1.316)}{0.7307} = 5,893$
Tube (item 1)	.3936	3273.6	1.316	$SEA_t = \frac{(3273.6)(1.316)}{0.3936} = 10,950$

TABLE III.- EFFECT OF SYSTEM MODIFICATIONS ON MEAN CUTTING FORCE

Combination	Number of drops averaged	Material	Typical shearing strength (ref. 7), psi	Number of cutters	Ensemble mean of mean wall thickness, in.	Ensemble mean of mean cutting force, lb	Ensemble mean, γ	Max. γ	Tube length (including end fittings), in.
1	13	2024-T3	41,000	20	0.0351	3273.6	1.081	1.160	21.75
2	9	2024-T3	41,000	20	.0357	3401.3	1.090	1.227	12.75
3	10	2024-T3	41,000	15	.0349	2653.4	1.110	1.217	21.75
4	13	2024-T3	41,000	15	.0356	2765.8	1.067	1.199	12.75
5	3	3003-H14	14,000	15	.0362	1536.0	1.097	1.212	21.75
6	2	3003-H14	14,000	15	.0352	1757.1	1.085	1.087	9.75

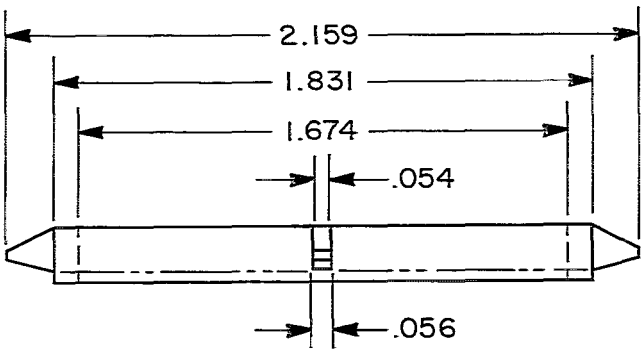

Side view

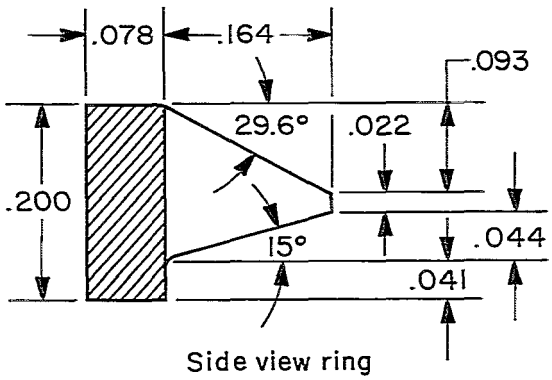

Side view ring and cutter cross section

Material: 4340 Steel

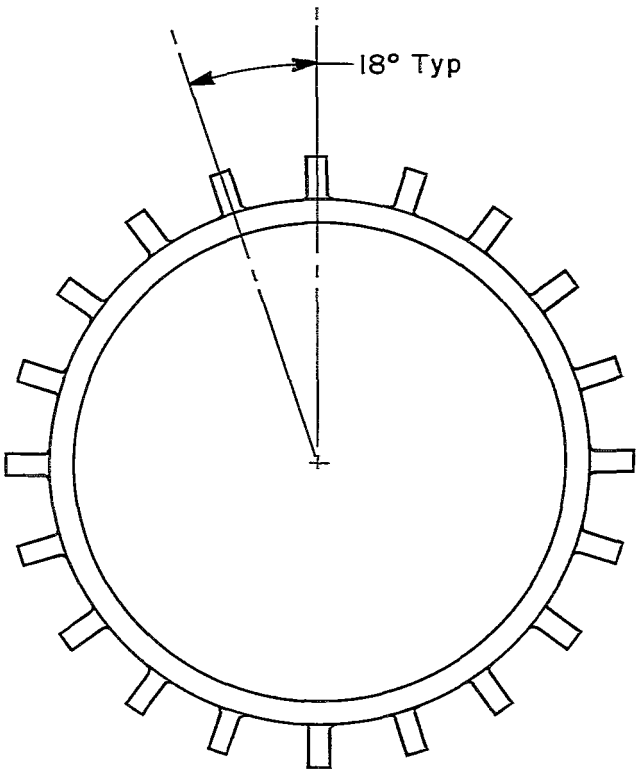

Top view cutting ring

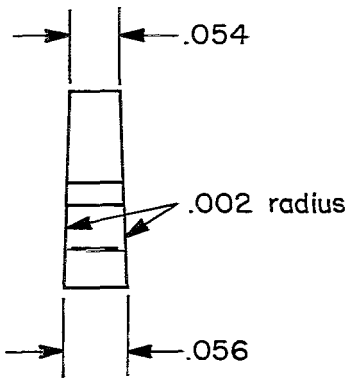

End view cutter

Note: All dimensions in inches

Figure 1.- Cutter ring.

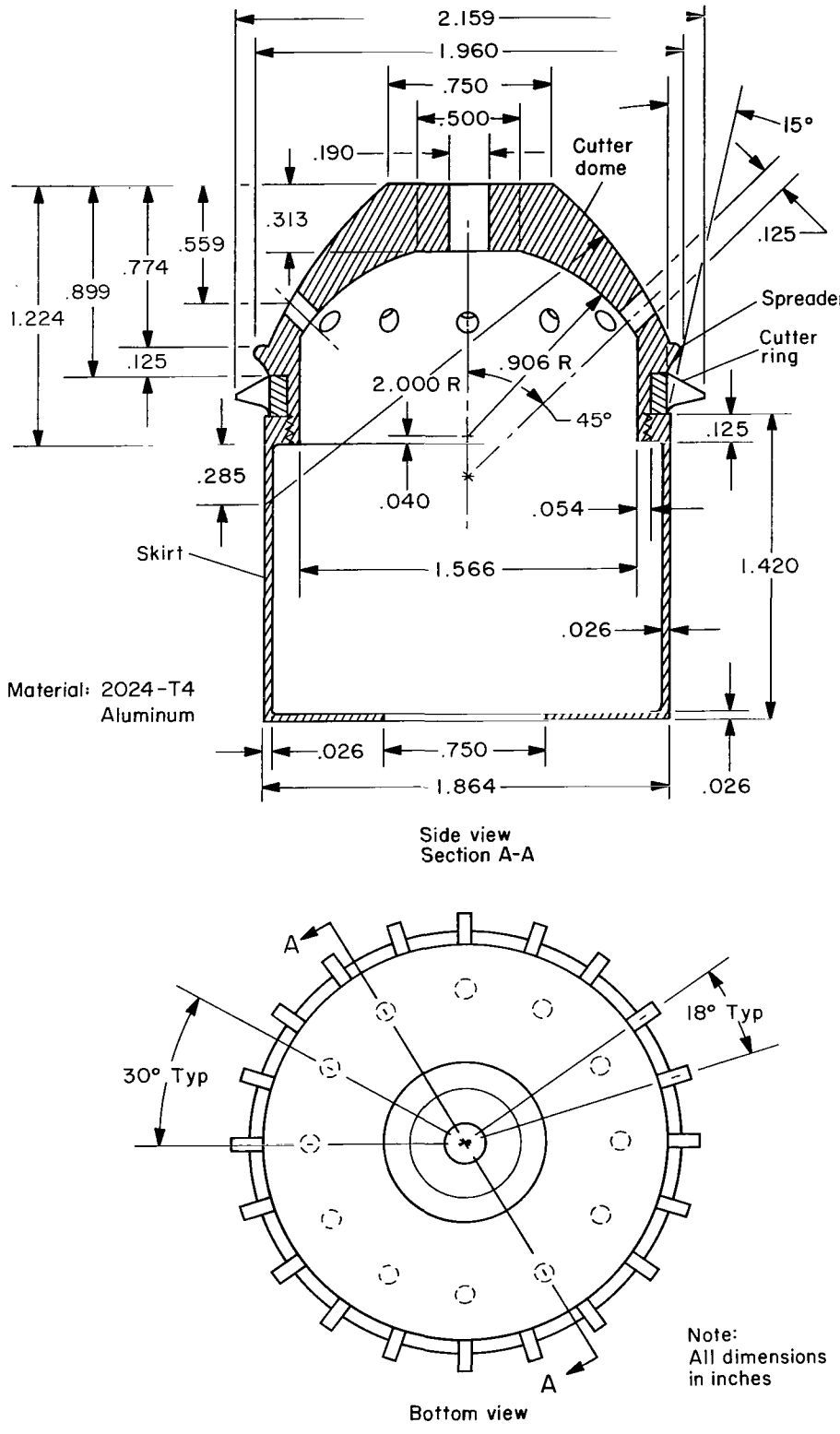

Figure 2.- Cutting dome.

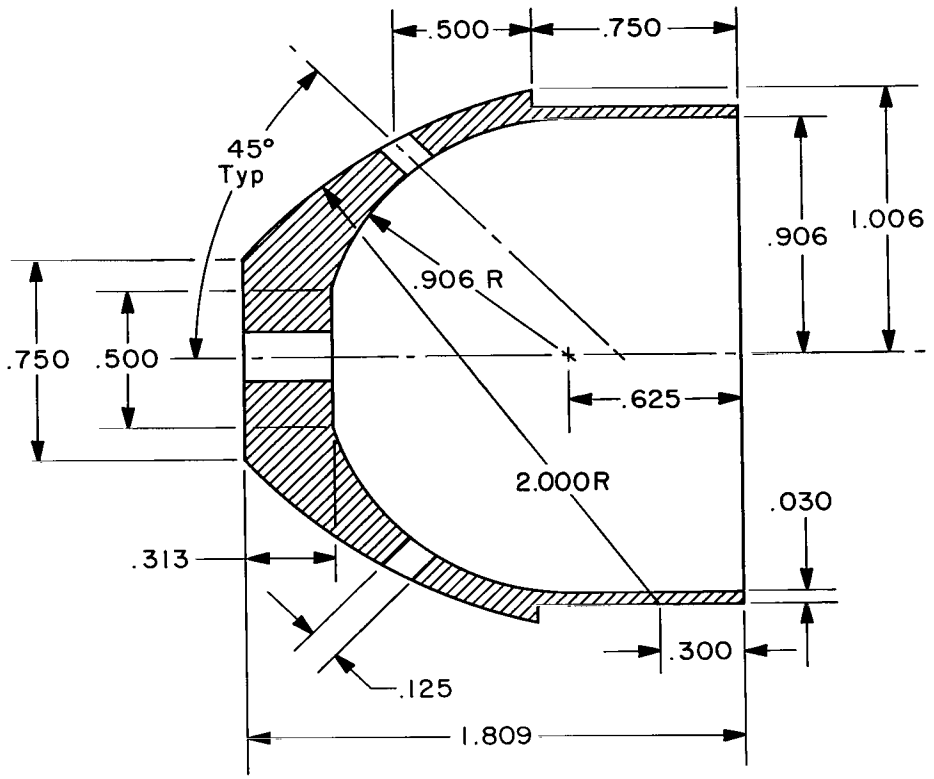

Side view
Section A-A

Material: 2024-T4
Aluminum

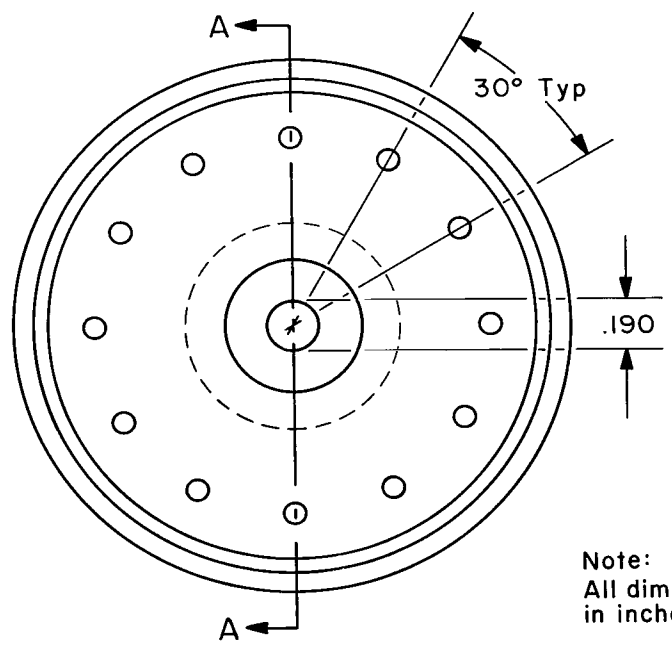

Bottom view

Note:
All dimensions
in inches

Figure 3.- Noncutting dome.

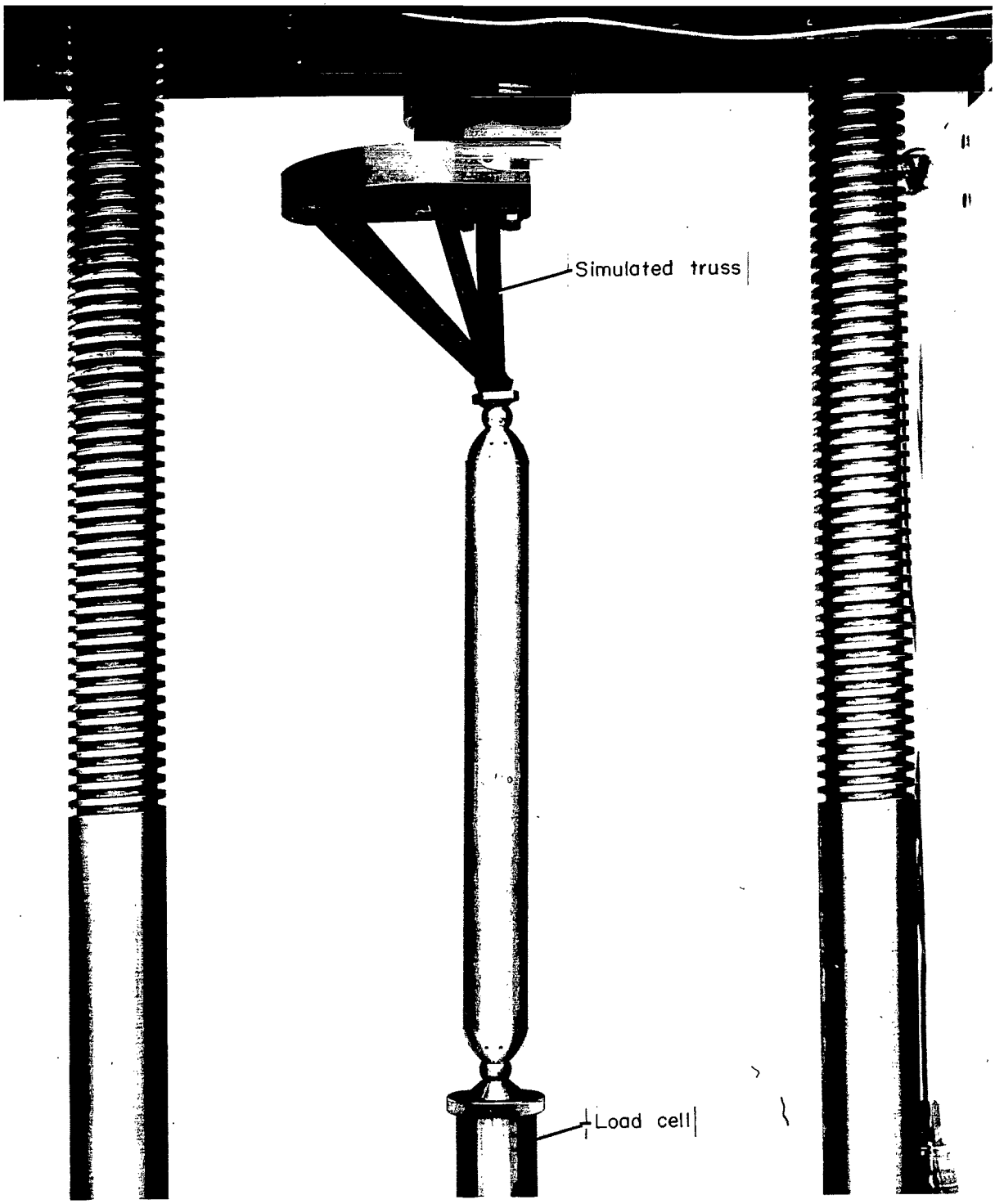

Figure 4.- Arrangement for static buckling or cutting test.

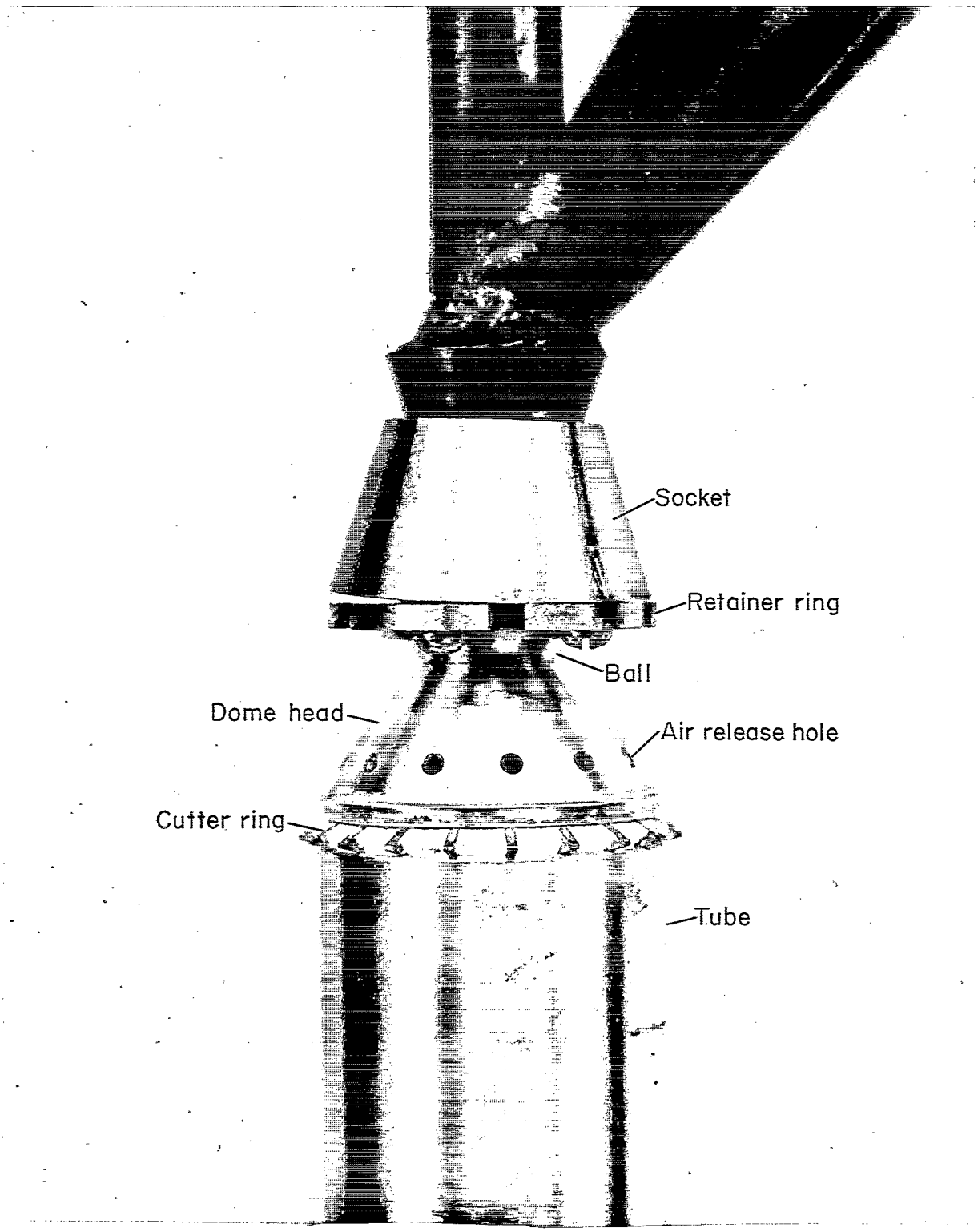

A-38727.1

Figure 5.- Cutting end of final assembled model.

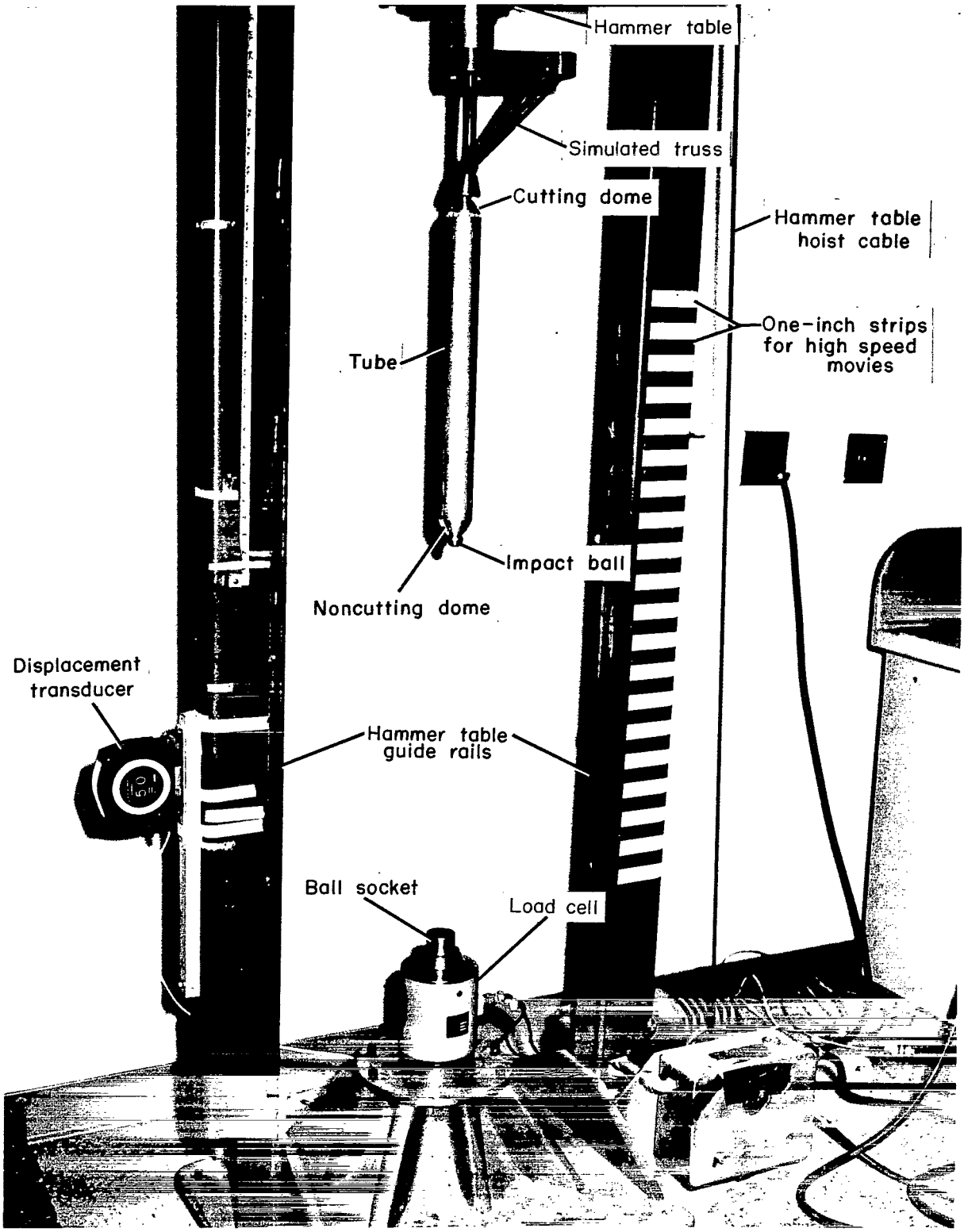

A-38728.1

Figure 6.- Cutter model prior to drop test.

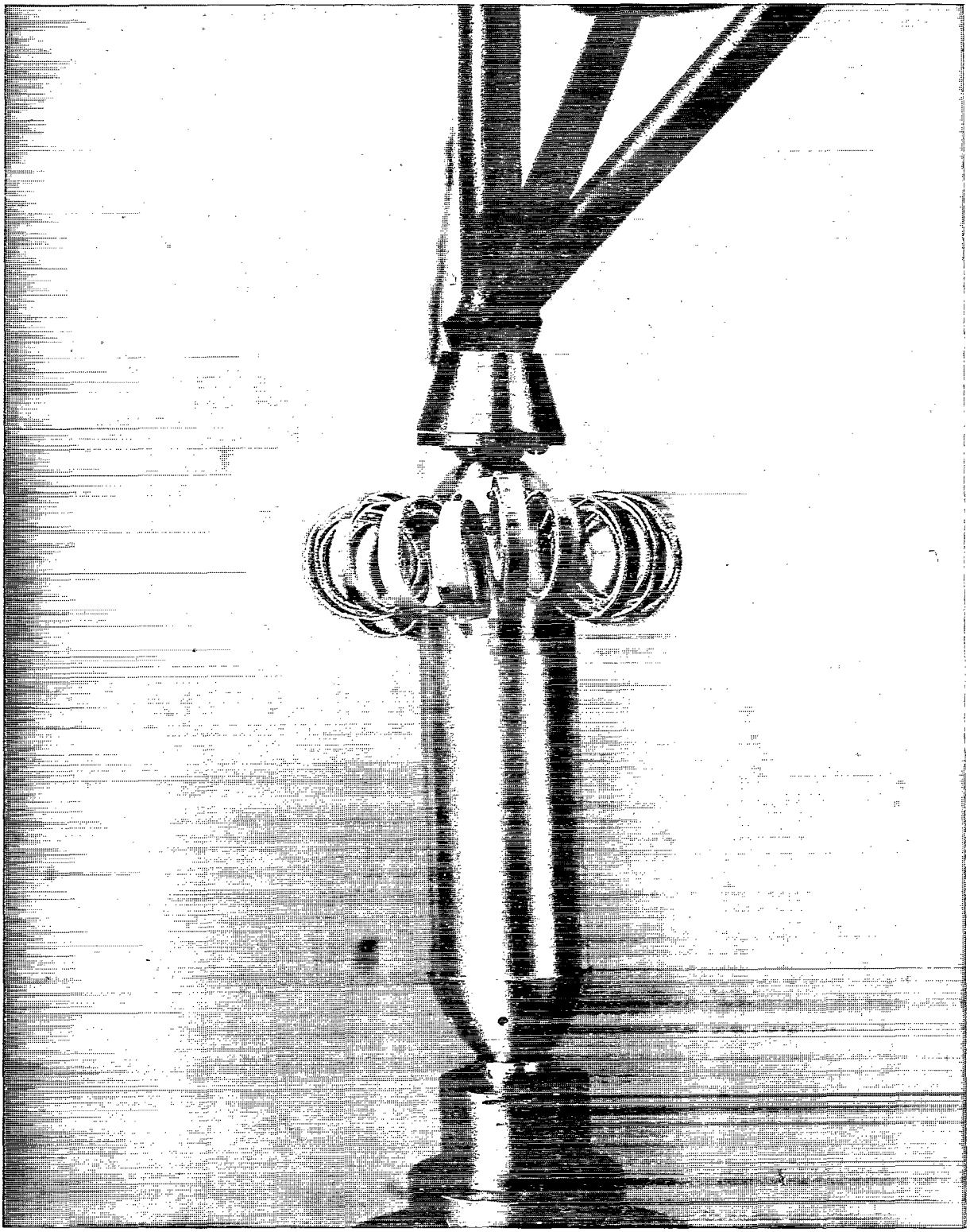

A-38729

Figure 7.- Cutter model after drop test.

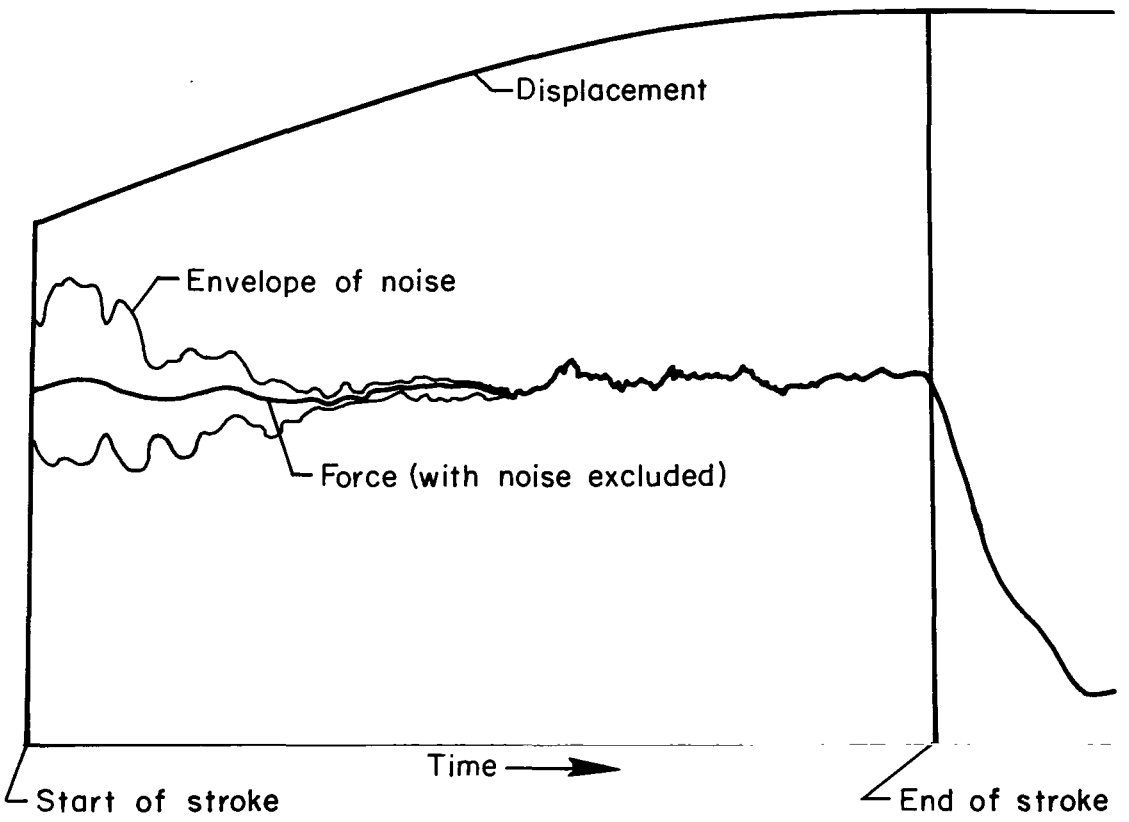

(a) Estimated impact velocity of 11.5 ft/sec, mean wall thickness of 0.0353 in. without precut (case 4 of table I).

Figure 8.- Drop-test records of force and displacement vs. time.

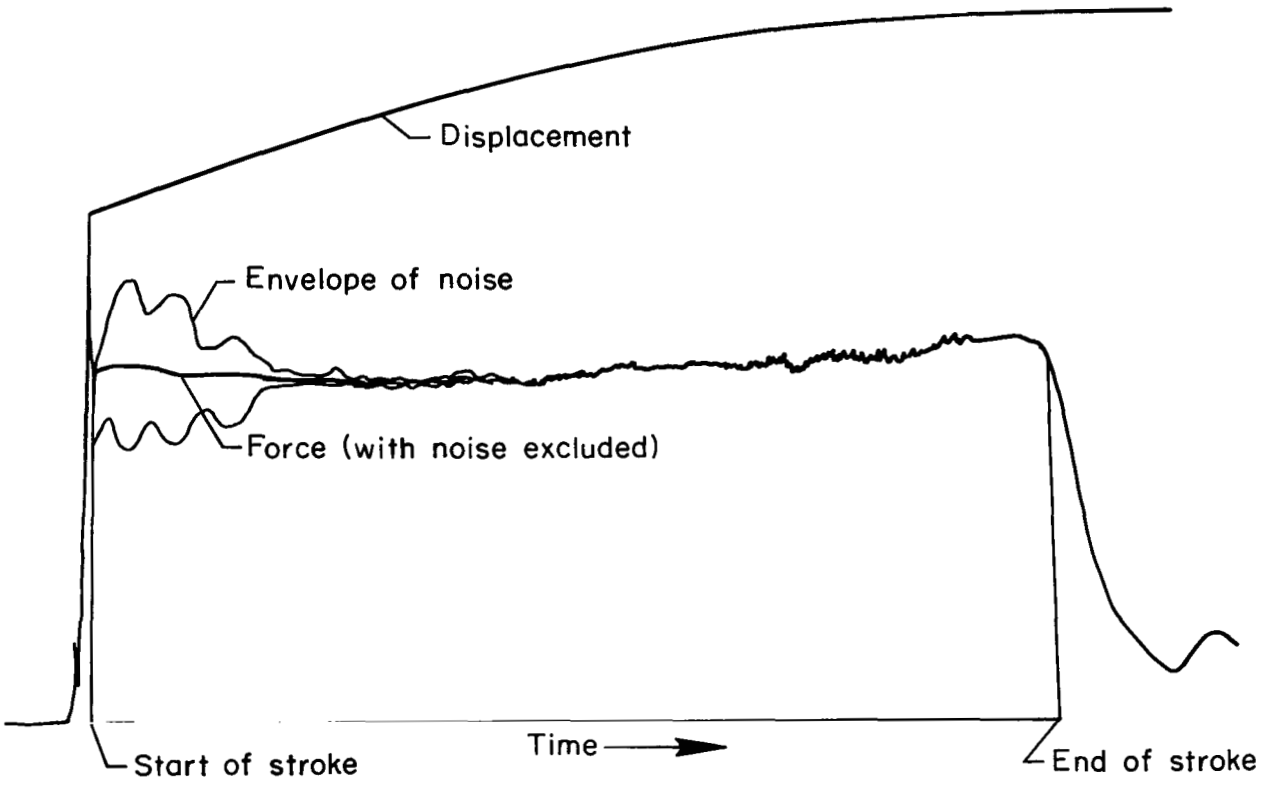

(b) Estimated impact velocity of 11.9 ft/sec, mean wall thickness of 0.0347 in. with precut (case 7 of table I).

Figure 8.- Continued.

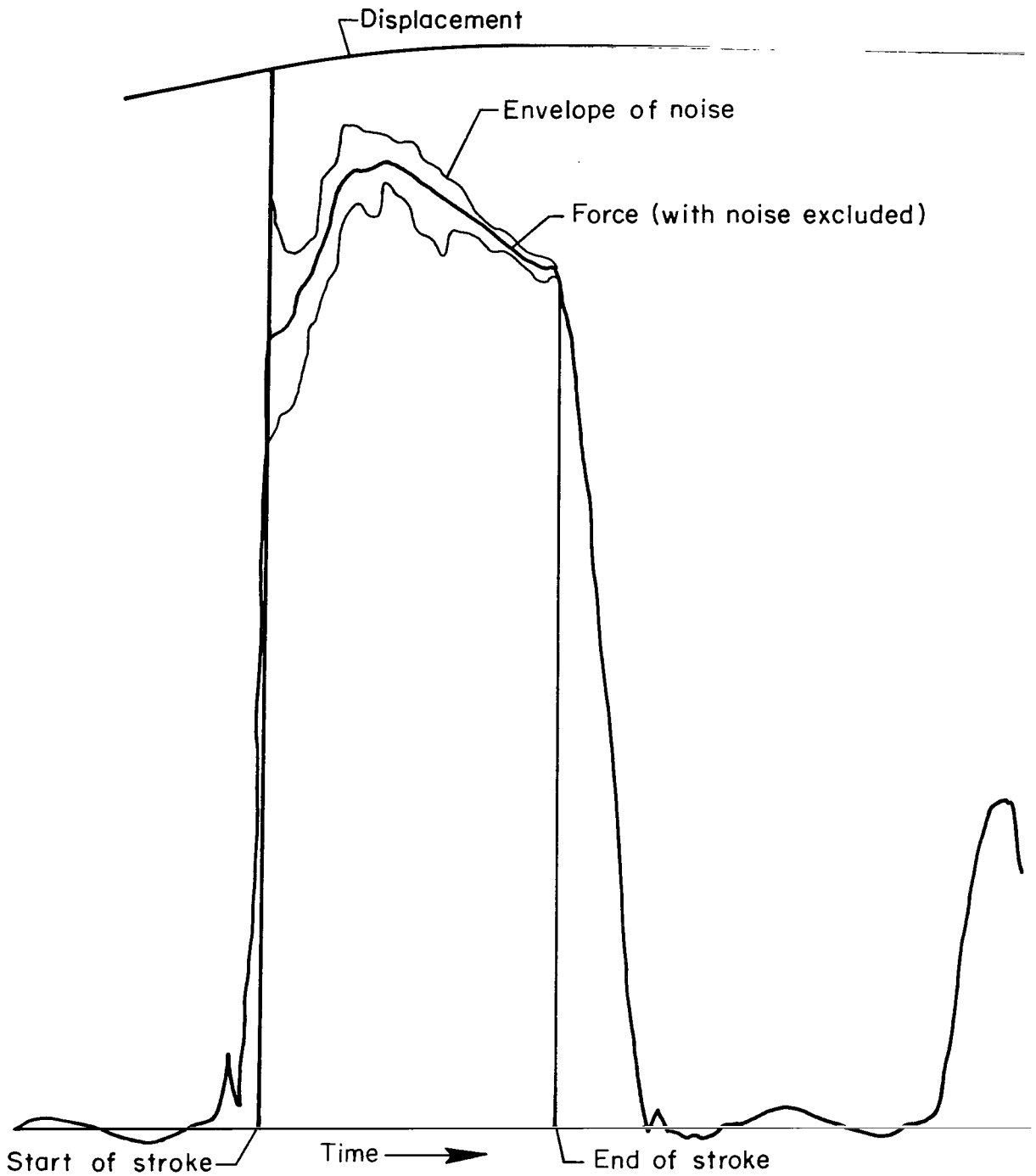

(c) Estimated impact velocity of 3.7 ft/sec, mean wall thickness of 0.0348 in. without precut (case 11 of table I).

Figure 8.- Continued.

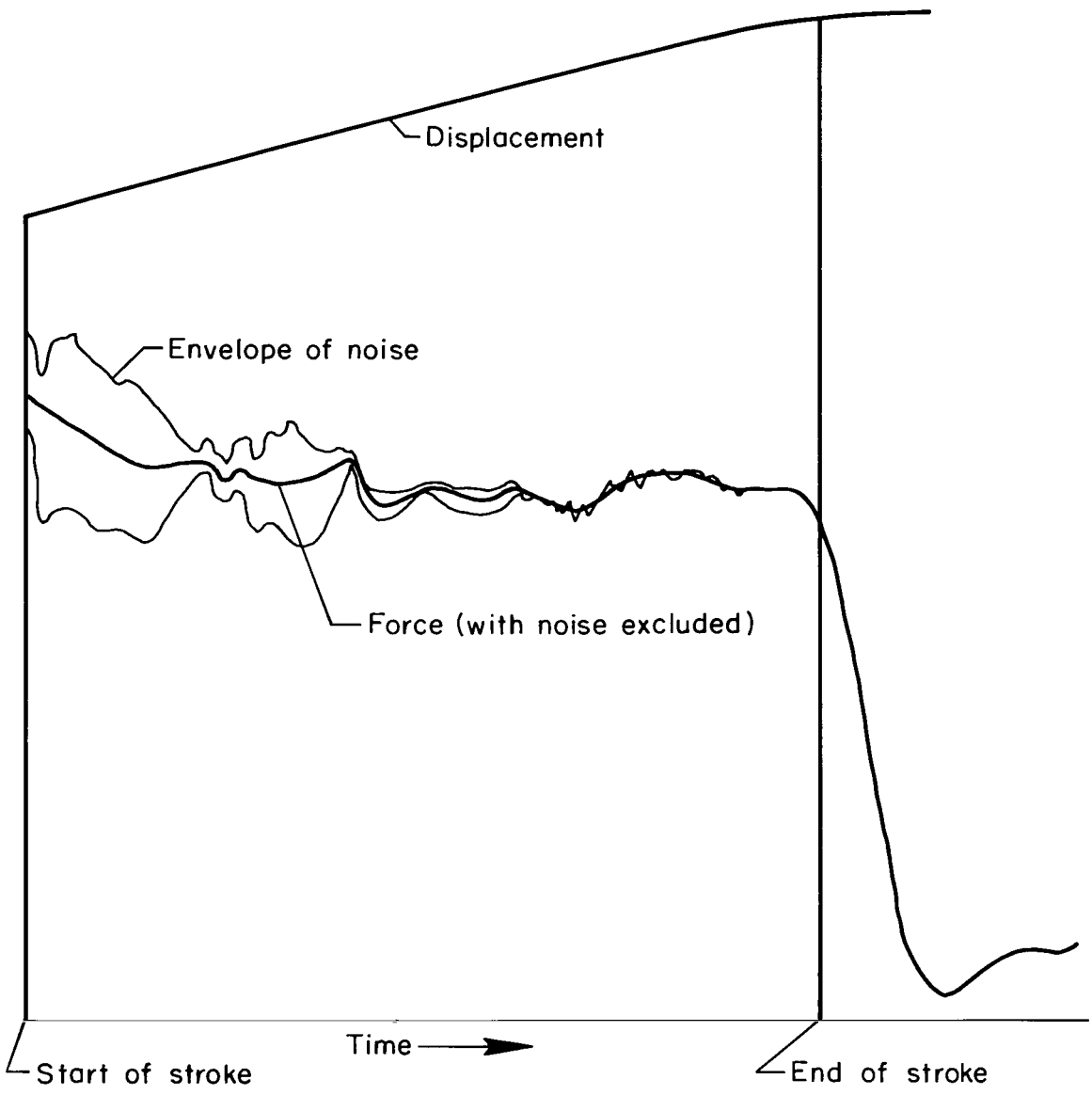

(d) Estimated impact velocity of 7.5 ft/sec, mean wall thickness of 0.0355 in. with precut (case 9 of table I).

Figure 8.- Concluded.

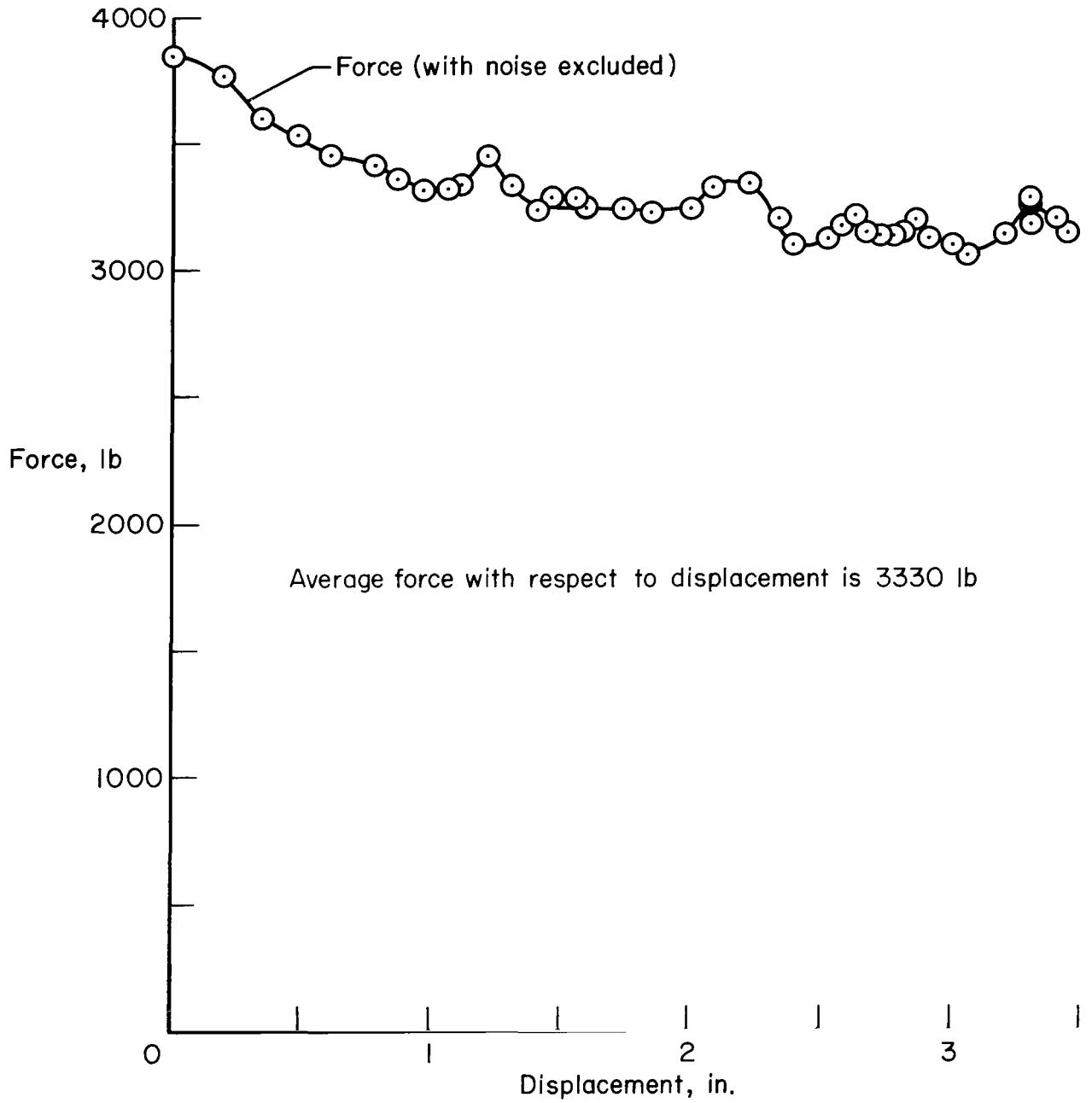

Figure 9.- Force vs. displacement (crossplot of fig. 8(d)) for estimated impact velocity of 7.5 ft/sec, mean wall thickness of 0.0355 in. with precut (case 9 of table I).

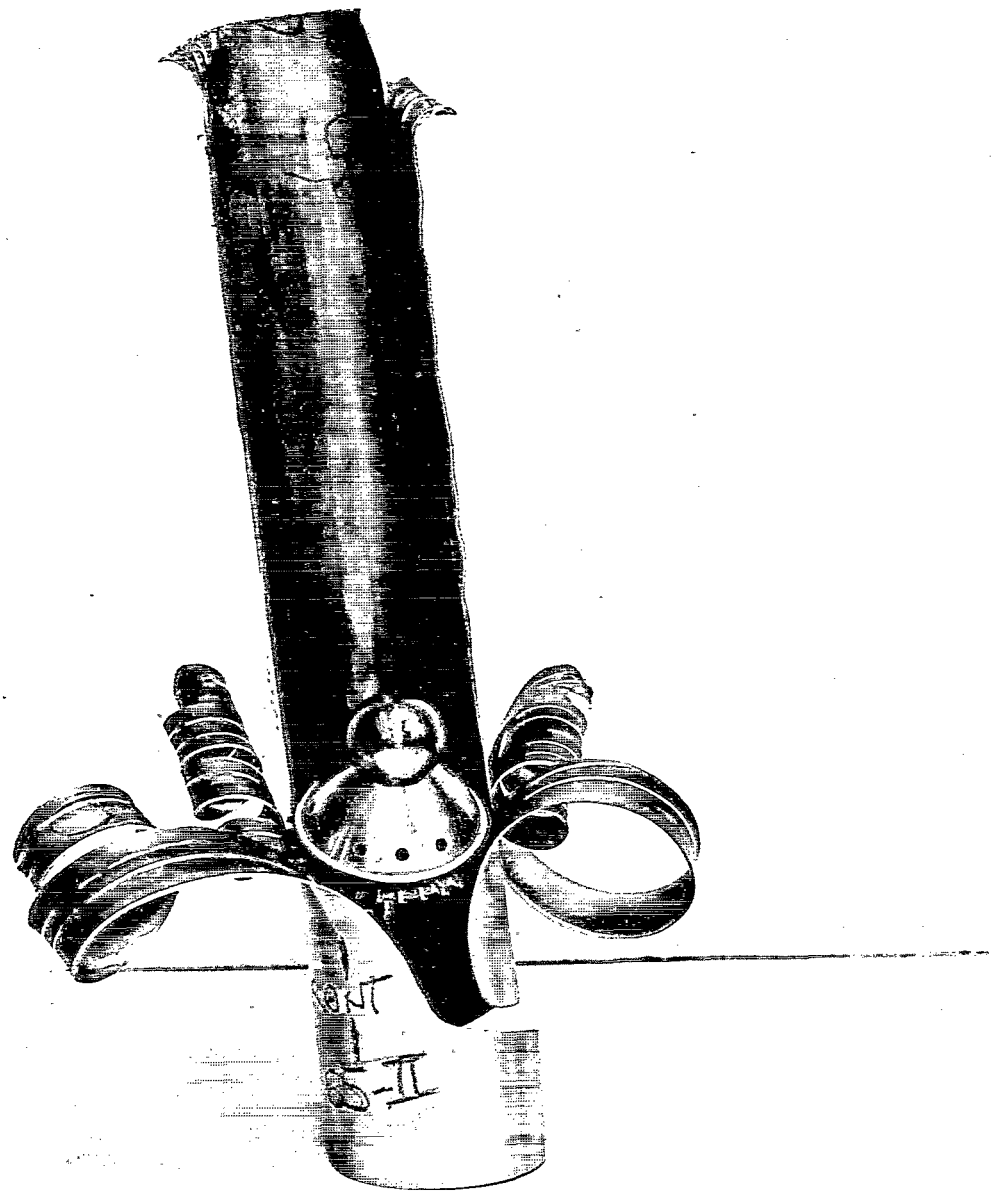

A-38731

Figure 10.- Catastrophic result of drop test for 2024-T3 tube.

A-38732

Figure 11.- Catastrophic result of drop test for 3003-H14 tube.

NASA-Langley, 1968 —— 32 A-2891

NATIONAL AERONAUTICS AND SPACE ADMINISTRATION
WASHINGTON, D. C. 20546

OFFICIAL BUSINESS

FIRST CLASS MAIL

POSTAGE AND FEES PAID
NATIONAL AERONAUTICS AND
SPACE ADMINISTRATION

POSTMASTER: If Undeliverable (Section 158 Postal Manual) Do Not Return

"The aeronautical and space activities of the United States shall be conducted so as to contribute . . . to the expansion of human knowledge of phenomena in the atmosphere and space. The Administration shall provide for the widest practicable and appropriate dissemination of information concerning its activities and the results thereof."

—NATIONAL AERONAUTICS AND SPACE ACT OF 1958

NASA SCIENTIFIC AND TECHNICAL PUBLICATIONS

TECHNICAL REPORTS: Scientific and technical information considered important, complete, and a lasting contribution to existing knowledge.

TECHNICAL NOTES: Information less broad in scope but nevertheless of importance as a contribution to existing knowledge.

TECHNICAL MEMORANDUMS: Information receiving limited distribution because of preliminary data, security classification, or other reasons.

CONTRACTOR REPORTS: Scientific and technical information generated under a NASA contract or grant and considered an important contribution to existing knowledge.

TECHNICAL TRANSLATIONS: Information published in a foreign language considered to merit NASA distribution in English.

SPECIAL PUBLICATIONS: Information derived from or of value to NASA activities. Publications include conference proceedings, monographs, data compilations, handbooks, sourcebooks, and special bibliographies.

TECHNOLOGY UTILIZATION PUBLICATIONS: Information on technology used by NASA that may be of particular interest in commercial and other non-aerospace applications. Publications include Tech Briefs, Technology Utilization Reports and Notes, and Technology Surveys.

Details on the availability of these publications may be obtained from:

SCIENTIFIC AND TECHNICAL INFORMATION DIVISION

NATIONAL AERONAUTICS AND SPACE ADMINISTRATION

Washington, D.C. 20546